Numerical Study of Adsorption for Fluids Mixture near Critical Point in a Micro-cavity

H. Smahi[a], D. Ameur[b], J. Dib[c], I. Raspo[d]

a.Laboratory of Theoretical Physics, Faculty of Sciences, University of Tlemcen, Algeria, housseynsmahi@gmail.com
b.Laboratory of Theoretical Physics, Faculty of Sciences, University of Tlemcen, Algeria, d.ameur@yahoo.fr
c.Laboratory of Theoretical Physics, Faculty of Sciences, University of Tlemcen, Algeria, joannadib2022@yahoo.fr
d.Aix-Marseille Université, CNRS, Centrale Marseille, M2P2 UMR7340, Marseille, France, isabelle.raspo@univ-amu.fr

Résumé:

L'objectif principal de cet article est l'étude d'une réaction d'adsorption et des transferts de masse associés dans un mélange binaire près du point critique du solvant. Le modèle physique consiste en un mélange dilué (naphtalène-CO_2supercritique) contenu dans une cavité rectangulaire d'une hauteur de l'ordre de 1 mm et présentant sur sa paroi inférieure une plaque chauffée et adsorbante. Pour tirer parti des propriétés spécifiques du fluide supercritique et optimiser les conditions thermodynamiques permettant une meilleure adsorption avec un bon transfert de masse, les effets de la proximité du point critique et du chauffage font l'objet de plusieurs simulations numériques dans le présent travail. Le modèle mathématique utilisé est basé sur la résolution des équations de Navier-Stokes, couplées aux équations d'énergie et de diffusion des espèces ainsi qu'à l'équation d'état de Peng-Robinson. Afin de réduire les coûts de calcul, ces équations sont résolues dans le cadre de l'approximation à faible nombre de Mach. Le champ de vitesse, la perturbation de la fraction massique ainsi que l'évolution temporelle du nombre moyen de Sherwood sont présentés pour différents chauffages. L'effet de confinement est également analysé. Les résultats montrent que, dans le voisinage du point critique du mélange et pour un fort chauffage de la paroi, on obtient l'adsorption homogène du soluté.Parmi les autres résultats clés, citons que, dans les mêmes conditions optimisées, le transfert de masse sur la plaque adsorbante est meilleur.

Abstract:

The main goal of this paper is the study of adsorption and mass transfer in a binary mixture near the solvent's critical point. The physical model consists of a dilute mixture (naphthalene-supercritical CO_2) enclosed in a rectangular cavity of height of order 1 mm with a hot and adsorbent plate at the bottom wall. To benefit from the supercritical fluid specific properties and optimize thermodynamics conditions allowing a better adsorption with a good mass transfer, effects of the critical point proximity and heating are the object of several numerical simulations in the present work. The mathematical model used is based on the solution of the Navier-Stokes equations, coupled with energy and mass diffusion equations with the Peng-Robinson equation of state. In order to reduce computational costs, these equations are solved in the low Mach approximation. The velocity field,

perturbation of the mass fraction as well as the temporal evolution of the average Sherwood number are presented for different heatings. The confinement effect is also analysed. The results show that in the mixture critical point neighborhood and for a very high heated wall, the homogeneous adsorption of the solute is obtained. Among other key results, we cite that, under the same optimized conditions, the mass transfer on the adsorbent plate is better.

Mots clefs : Adsorption, mass transfer, microfluidic, supercritical mixture, Piston effect.

1 Introduction

Adsorption allows a selective transfer of species from fluid phase to a solid adsorbent. When an adsorbent is exposed to a fluid phase, the molecules of the fluid phase diffuse on its surface. The type of adsorption isotherm of a particular system can provide a source of information on the surface characteristics and pore properties of the adsorbent.The reversible type isotherm is obtained when the adsorption is limited to a few molecular layers. This condition is generally met for adsorption on microporous materials having small external surfaces such as activated carbons.

Adsorption from supercritical fluids on surfaces or inner surfaces of porous particles is more complex. Very close to the critical temperature, the adsorption isotherm can exhibit a sharp spike near the critical pressure while a decrease of the excess amount adsorbed is observed for larger pressures [1]. Adsorption on activated carbon can be associated with Supercritical Fluid Extraction (SFE) for soil remediation. The SFE process has already been used in soil remediation using both propane and CO_2 as a solvent [2]. It was applied to organic compounds of different chemical nature, mainly high molecular weight hydrocarbons [3]. The extraction of various organics like naphthalene, anthracene, hexachlorobenzene, and phenol from soil using supercritical carbon dioxide has been reported [4,5]. Environmental legislation demands low concentration of contaminants in the soil and therefore, when supercritical solvent is recirculated, the process has to be almost free of contaminant. With volatile pollutants, separation of solvent and solute by decompression is not efficient enough to reach the required low concentration in the soil and a second step of adsorption onto activated carbon is needed. In this context, Madras et al. [6] proposed a process combining supercritical extraction and adsorption for remediation of soils contaminated with heavy molecular weight organic compounds [7]. The organic pollutants are continuously extracted using supercritical carbon dioxide and then deposited on activated carbon. It was found that the process would operate in the optimum mode if the desorption of soil was performed at low temperatures followed by adsorption at high temperatures [8].

A few theoretical or numerical studies were performed on adsorption from supercritical fluids. Lucas et al. [9] proposed a model taking into account equilibrium (adsorption isotherm), diffusion in the solid (effective diffusion coefficient), mass transfer from the bulk of the fluid phase (supercritical solvent) to the surface of the solid, axial dispersion (effective dispersion coefficient) and a first order reversible adsorption/desorption reaction at the solid surface site. The three-parameter model proposed for supercritical CO_2 adsorption on activated carbon is able to adjust the experimental data (ethyl acetate for example) with a mean deviation lower than 8%. For a generic heterogeneous reaction (relevant for adsorption/desorption), Raspo et al. [10] showed by numerical simulations that the hydrodynamic behavior of supercritical fluids can couple with the critical behavior of the solubility of solids to trigger the reaction in dilute binary supercritical mixtures. More precisely, by heating the

mixture at one side, the Piston effect (through the strong and homogeneous increase of pressure that it provokes in the whole fluid) causes the release of a heterogeneous reaction at the opposite plate that was kept at the initial temperature [10, 11]. Wannassi and Raspo [12] investigated the adsorption in a model binary mixture, the naphtalene-CO_2 mixture, near the solvent's critical point in a side-heated cavity. The diverging behavior of the equilibrium constant and the Piston effect were taken into account and their influence on the adsorption process is highlighted. The results showed that, very close to the critical point, the increase of the wall heating remarkably affects the adsorbed amount at the two reactive boundaries and the mass fraction inside the cavity [12].

To design an adsorption plant, it is necessary to have reliable mass-transfer models that allow the determination of optimum operating conditions and the scale-up. Nevertheless, few attempts have been performed to model the supercritical adsorption process [8, 9, 13] and most of the efforts have been focused on supercritical fluid extraction [14]. In this paper, adsorption of a model solute from supercritical CO_2 is investigated in a small side-heated cavity by means of 2D numerical simulations. Naphthalene was chosen as a model solute because its phase equilibria with CO_2 has been thoroughly studied [10-11]. The effects of heating and confinement are discussed. The results show a strong influence of the cavity height.

2 Physical and mathematical model

The physical model consists of a dilute mixture (Naphthalene-CO_2) enclosed in a rectangular cavity of aspect ratio L/H=10 with a heated and adsorbent plate on a part of the bottom boundary as shown in figure 1. Two cavity heights H are considered: 1 and 0.5mm. An adiabatic boundary condition is applied on the non-reactive vertical walls. At time t=0, the fluid is considered in thermodynamic equilibrium at a constant temperature T_i slightly above a particular mixture critical temperature T_{cm}= 307.65K (T_i= (1+ ε)) and stratified with the mean density equal to the mixture critical density ρ_{cm}=470kg.m^{-3}.The parameterε = (T_i-T_{cm})/T_{cm} defines the dimensionless proximity to this mixture critical point named the Lower Critical End Point (LCEP) that is slightly above the critical point of CO_2. A weak heating is then gradually applied at the solid bottom plate defined by$H<x<L-H$. The temperature increases ΔT vary from 10mK up to 100mK.

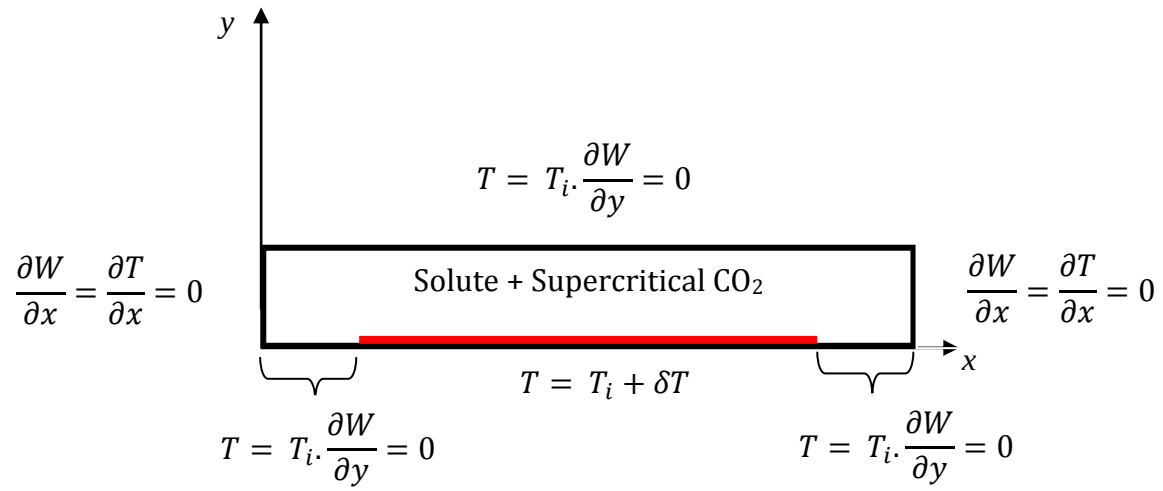

FIGURE 1: Physical configuration

The phase diagram of binary mixtures of interest for SFE and adsorption exhibits a discontinuous mixture critical line (Fig. 2). The low temperature part ends at the LCEP that is the junction between the solid–liquid–vapor coexistence line and the mixture critical line starting at the critical point of the solvent (species 1). In the same way, the high temperature part starts at the critical point of the solute (species 2) and ends at the UCEP. For temperatures between T_{LCEP} and T_{UCEP}, the mixture exhibits an equilibrium between a solid phase of the solute only and a fluid phase of the mixture.

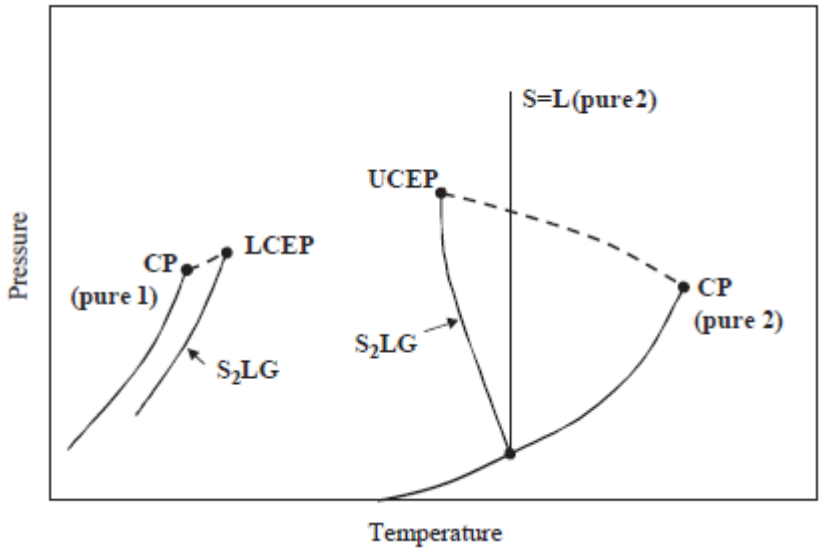

FIGURE 2 : Phase diagram of binary mixtures of interest (CP: critical point; LCEP: Lower Critical End Point; UCEP: Upper Critical End Point; S=L: solid–liquid equilibrium curve; S_2LG: solid–liquid–gas curve; dotted lines: liquid–gas critical lines of the mixture).

Near the LCEP, the solubility of solids and the equilibrium constant of adsorption are very sensitive to variations of temperature and pressure. That is the reason why SFE and adsorption processes are usually performed in this region of the phase diagram. On the other hand, the derivative of the equilibrium constant with respect to pressure diverges as approaching the LCEP. As shown in [12], this divergent behavior, coupled with the Piston effect, can induce a decrease in the adsorbed amount for increasing heating of the boundary.

The Naphthalene-CO_2 mixture was chosen as a reference system with the above-mentioned phase diagram because of the wide experimental data on solubility that can be found in literature, allowing an easier validation of the thermodynamic model [12]. The physical properties of each pure compound are given in Table 1. We consider a dilute mixture of Naphthalene (the minority species) and supercritical CO_2. Naphthalene is the species adsorbed on the bottom plate.

	T_c (K)	ρ_c (kg.m^{-3})	M (kg.mol^{-1})	ω
CO_2 (1)	304.21	467.8	4.401×10^{-2}	0.225
Naphthalene (2)	748.40	314.9	1.282×10^{-1}	0.302

Table 1 : Pure component properties (critical temperature and density T_c and ρ_c, molecular weight M and acentric factor ω).

The mathematical model is based on the 2D time-dependent and compressible Navier–Stokes equations, coupled with energy and mass diffusion equations and the Peng–Robinson equation of state. In order to reduce computational costs, these equations are solved in the framework of the low Mach number approximation [15]. Thus, the total pressure P is split into two parts: a homogeneous thermodynamic part $P_{th}(t)$, which appears in the equation of state and in the energy equation and only depends on time t, and a non-homogeneous dynamic part $P_{dyn}(x, y, t)$, appearing in the momentum equation and which varies with time and space. We use the modification of the low Mach number approximation proposed by Accary et al [16] to account for the strong stratification in fluids near the critical point. We chose T_{cm} as characteristic temperature, ρ_{cm} as characteristic density, H as characteristic length, the Piston effect time scale t_{PE} [10-12] as characteristic time and the corresponding velocity $V_{PE}=H/t_{PE}$ as characteristic velocity. The dimensionless governing equations are therefore:

$$\frac{\partial \rho}{\partial t} + \frac{\partial}{\partial x}(\rho V) = 0 \tag{1}$$

$$\rho \frac{\partial V}{\partial t} + \rho V.\nabla V = -\nabla P_{dyn} + \frac{1}{Re}\Delta V + \frac{1}{3Re}\nabla(\nabla.V) + \frac{1}{Fr}(\rho - \rho_i) \tag{2}$$

$$\begin{aligned}\rho \frac{\partial T}{\partial t} + \rho V.\Delta T = &-\frac{C_{V0}}{C_{Vi}}(\gamma_0 - 1)T\left(\frac{\partial P_{th}}{\partial T}\right)_{\rho,w}(\nabla.V) + \frac{\gamma}{RePr}\nabla.(\lambda^*\nabla T) \\ &+ \frac{1}{(\gamma-1)^2 Le}\nabla.\left[\left((\bar{U}_2^* - \bar{U}_1^*) + \frac{C_{V0}}{C_{Vi}}(\gamma_0 - 1)P_{th}(\bar{V}_2^* - \bar{V}_1^*)\right)\rho D_{21}^*\nabla w\right] \\ &- \frac{1}{(\gamma-1)^2 Le}\left[(\bar{U}_2^* - \bar{U}_1^*) + \frac{C_{V0}}{C_{Vi}}(\gamma_0 - 1)\left(P_{th} - T\left(\frac{\partial P_{th}}{\partial T}\right)\right)_{\rho,\omega}(\bar{V}_2^* - \bar{V}_1^*)\right]\nabla.(\rho D_{21}^*\nabla w)\end{aligned} \tag{3}$$

$$\rho \frac{\partial w}{\partial t} + \rho V.\nabla w = \frac{1}{(\gamma-1)^2 Le}\nabla.(\rho D_{21}^*\nabla w) \tag{4}$$

In the above equations, V is the velocity of components u and v in the x- and y-directions respectively, w is the mass fraction, γ is the ratio of the isobaric C_p and isochoric C_v specific heats calculated from the equation of state, γ_0 and C_{v0} correspond to the values for a perfect gas (γ_0= 1.3, C_{v0}= 3R/M$_1$) and the subscript i refers to values at the initial condition. The dimensionless parameters are the Mach number *Ma*, the Reynolds number *Re*, the Froude number *Fr*, the Prandtl number *Pr* and the Lewis number *Le* and are respectively defined by:

$$Ma = \frac{V_{PE}}{C_0} \quad ; \quad Re = \frac{\rho_i V_{PE} H}{\mu_i} \quad ; \quad Fr = \frac{V_{PE}^2}{gH} \quad ; \quad Pr = \frac{\mu_i \gamma C_{Vi}}{\lambda_i} \quad ; \quad Le = \frac{\lambda_i}{\rho_i \gamma C_{Vi}(D_{21})_i}$$

where $c_0 = \sqrt{\gamma_0\left(\frac{R}{M_1}\right)T_{cm}}$ is the sound speed.

In Eq. (3), $\overline{U_k^*}$ and $\overline{V_k^*}$ are respectively the dimensionless partial molar internal energy and partial molar volume expressed as follows:

$$\overline{U_k^*} = \overline{U_k}/(M_2 C_{vi} T_{cm}) \text{ and } \overline{V_k^*} = \overline{V_k}/(M_2/\rho_i) \text{ for k=1, 2}$$

with $\overline{U_k}$ and $\overline{V_k}$ the partial molar internal energy and partial molar volume, respectively, calculated from the Peng-Robinson equation [12].

As we consider dilute mixtures, the thermal conductivity λ and the dynamic viscosity μ of the mixture are supposed to be those of the pure CO_2. We use the values given by the NIST for μ and the

correlation of Arai et al. [17] for λ. The binary mass diffusion coefficient D_{21} is modeled using the Wilke-Chang equation [18].

The thermodynamic state of the mixture is described by thePeng–Robinson equation of state in the framework of the one-fluid theory:

$$\boldsymbol{P_{th}} = \frac{\boldsymbol{T\rho\theta(w)}}{\boldsymbol{1-b^*(w)\rho/\theta(w)}} - \frac{\boldsymbol{a^*(T,w)\rho^2}}{\boldsymbol{1+2b^*(w)\rho/\theta(w)-b^*(w)^2\rho^2/\theta(w)^2}} \quad (5)$$

Where:

$\theta(w)=1-\left(1-\frac{M_1}{M_2}\right)w$

$$a^*(T,w) = a^*_1(T)(1-w)^2 + 2a^*_{12}(T)w(1-w) + a^*_2(T)w^2,$$

$$b^*(w) = b^*_1(1-w)^2 + 2b^*_{12}w(1-w) + b^*_2w^2,$$

$$a^*_1(T) = 1.487422\frac{T_{c1}}{T_{cm}}\frac{\rho_i}{\rho_{c1}}\left[1+\beta_1\left(1-\sqrt{T(T_{cm}/T_{c1})}\right)\right]^2$$

$$a^*_2(T) = 1.487422\frac{M_1}{M_2}\frac{T_{c2}}{T_{cm}}\frac{\rho_i}{\rho_{c2}}\left[1+\beta_2\left(1-\sqrt{T(T_{cm}/T_{c2})}\right)\right]^2$$

$b^*_j = 0.253076\left(\frac{\rho_i}{\rho_{cj}}\right)$ with j=(1,2)

$$a^*_{12}(T) = \sqrt{a^*_1(T)a^*_2(T)}(1-k_{12}),$$

$$b^*_{12} = \frac{1}{2}\left(b^*_1\frac{M_1}{M_2} + b^*_2\right)(1-l_{12}),$$

$\beta_j = 0.37464 + 1.54226\omega_j - 0.26992\omega_j^2$ (j=1,2)

with ω the acentric factor (Table 1). The binary interaction parameters k_{12} and l_{12} are determined so as to minimize the error between the calculated and experimental solubility data [10]. The superscript (*) refers to dimensionless parameters.

On the adsorbent plate, the adsorption reaction is modeled by a first order reaction. In order to avoid discontinuities between the plate and the isothermal and non-reactive parts of the bottom boundary y=0, the following boundary conditions are prescribed for temperature T and mass fraction w:

$$T = T_i + \Delta T\Phi(x) \quad (6)$$

$$D_{21}\frac{\partial w}{\partial y} = K_a\Phi(x)w \quad (7)$$

where Φ(x) is a function allowing a continuous transition between the plate and the other parts of the boundary. It is defined by:

$$\Phi(x) = \left[\frac{th(2x-4)-th(-4)}{th(2L/H-4)-th(-4)}\right]\left[\frac{th(2L/H-2x-4)-th(-4)}{th(2L/H-4)-th(-4)}\right]$$

In Eq. (7), K_a is the adsorption equilibrium constant that depends on temperature and pressure. Since small temperature differences ΔT are considered, K_a is linearized as follows [14]:

$$\boldsymbol{K_a = K_{ai} + \left(\frac{\partial K_a}{\partial T}\right)_p(T-T_i) + \left(\frac{\partial K_a}{\partial P}\right)_T(P-P_i)} \quad (8)$$

3 Results

Simulations were performed for an initial temperature T_i=308.15K, which corresponds to a distance to the mixture critical point equal to 0.5K. Four values of the bottom plate heating were considered: ΔT=10, 20, 50, 100mK, respectively.The mixture is saturated, which means that the initial mass fraction w_i= 7.6751×10^{-3} corresponds to the solubility of Naphthalene in CO_2 at 308.15K. The values of the various properties and transport coefficients at the initial state are: μ_i = 3.3402×10^{-5}Pa.s^{-1}, λ_i = 9.6172×10^{-2} W.m^{-1}.K^{-1}, C_{Vi} = 1306.27 J.kg^{-1}.K^{-1}, $(D_{21})_i$ = 2.1969×10^{-8} m².s^{-1}, β_i = 2.3134×10^{-1} K^{-1}, γ = 16.75. As already said in section 2, since the binary mixture is very dilute because of the low solubility of the solute, we can assume that the transport coefficients of the mixture are those of the pure solvent. Thus, the thermal expansion coefficient β and the ratio of heat capacities γ were calculated from the Peng-Robinson equation for pure CO_2. For T_i=308K, the derivatives of the adsorption constant in Eq. (8) are $(\partial K_a/\partial T)$ = 0.295 and $(\partial K_a/\partial P)$ = -2.90×10^{-6}. The Damköhler number was fixed to $Da=HK_{ai}/(D_{21})_i=10^{-5}$, which is a pertinent value for an adsorption reaction.

3.1. Influence of the heating:

In this section, we present the system's response to the heating of the bottom plate. Figure 3 shows the isolines of temperature and mass fraction perturbation for the four values of heating ΔT. The times correspond to $5t_{PE}$ and $120t_{PE}$ for all the cases.

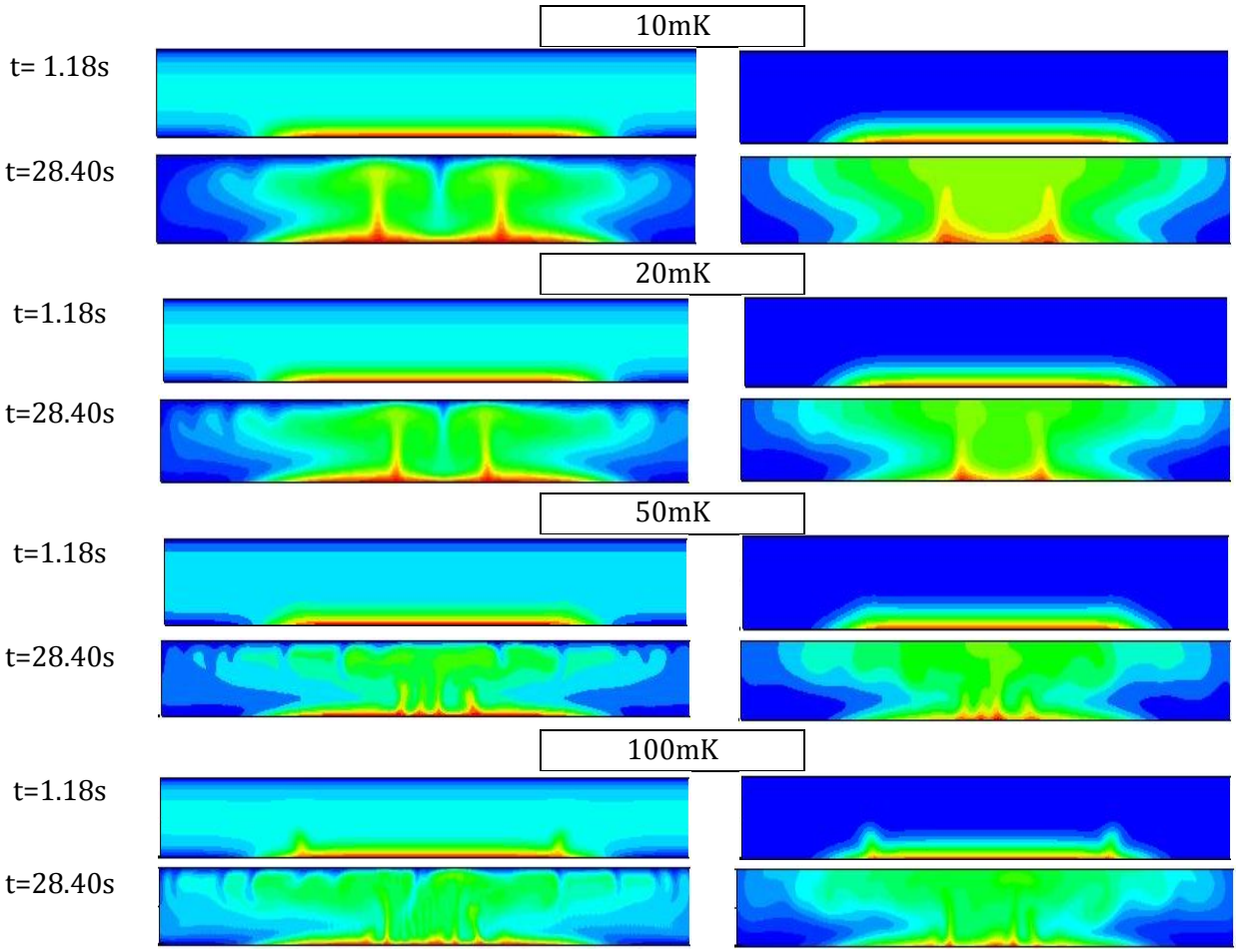

FIGURE3. Isolines of temperature (left column) and mass fraction perturbation w-w_i (right column) for the four values of ΔT (20, 30, 50 and 100mK respectively) for H=1mm.

The solutions obtained for the various values of ΔT at $5t_{PE}$ are similar. The temperature field at this time is governed by the Piston effect, as in pure CO_2 [16], with three distinct zones: a hot boundary layer along the heated plate, cold boundary layers along isothermal walls and the cavity bulk which is homogeneously heated by the Piston effect. The mass fraction perturbation just shows mass transfer by diffusion along the adsorbent plate. For t≥28.40s, the isoline map of the mass fraction does not evolve anymore. However,it must be underlined that w-$w_i$keeps on increasing while the adsorption reaction still goes on. As expected, for t=28.40s, the temperature field is very different depending on the ΔT. Indeed, because of the diverging behavior of the thermal expansion coefficient β, the Rayleigh number strongly increases with the heating: $Ra=3.4\times10^4$ for ΔT=10mK, $Ra=6.8\times10^4$ for ΔT=20mK, $Ra=1.7\times10^5$ for ΔT=50mK and $Ra=3.4\times10^5$ for ΔT=100mK. As a consequence, the convective flow is much more intense for ΔT=100mK, allowing a better mixing inside the cavity. The distribution of the convective cells directly affects the mass fraction field as it is revealed in figure 4 showing the velocity field together with the isolines of w-w_i. The jet flow between contrarotative rolls is much weaker for ΔT=10 and 20mK (Fig. 4.(a-b)). For ΔT=50 and 100mK (Fig. 4(c-d)), in contrast, the very intense convective cells restrict the diffusion of the solute in the boundary layer along the plate.

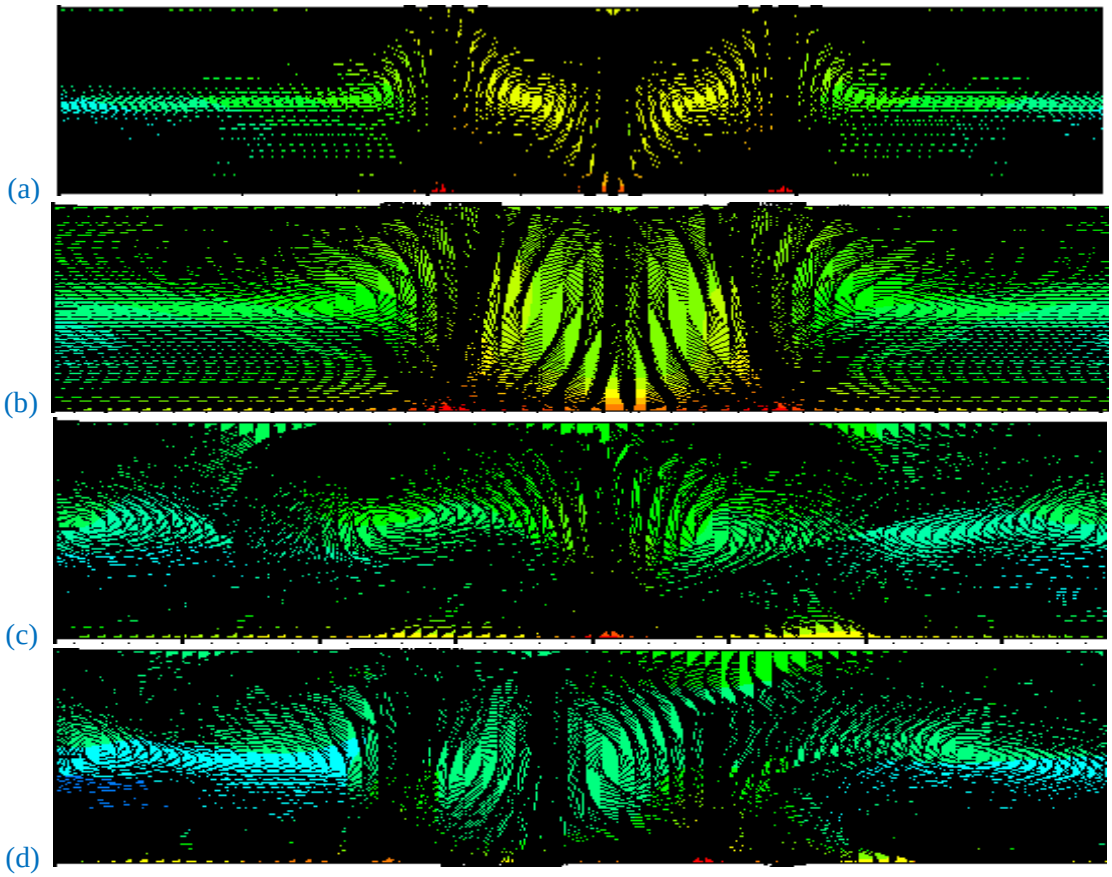

FIGURE4. Velocity field together with the isolines of w-$w_i$in the central part of the cavity (above the heated plate) for (a) ΔT=10mK, (b) ΔT=20mK, (c) ΔT=50mK and (d) ΔT=100mK, and for H=1mm.

The convection flow has also a strong influence on the adsorbed amount of solute. Figure 5 presents the profile of the relative mass fraction perturbation $(w\text{-}w_i)/w_i$ on the bottom boundary for the four ΔT. It reveals that the profile is more homogenous for large ΔT (50mK and 100mK) than for small ones. Therefore, in the framework of adsorption processes for example, a more homogeneous material can be obtained for large ΔT. On the other hand, the magnitude of adsorbed amount decreases when ΔT

increases. As was shown in [12], this decrease is due to the Piston effect, coupled with the divergent behavior of the derivative ($\partial K_a/\partial P$) that is negative andinduces a decrease of the adsorption constant (Eq. (8)). The larger ΔT *is*, the larger the pressure increase generated by the Piston effect is and the smaller the adsorption constant is. It must be noted that the divergence of infinite-dilution properties of the solute (that is responsible for the divergence of the adsorption equilibrium constant derivative) is not specific of Naphthalene but it is a universal behavior for dilute mixtures [12].

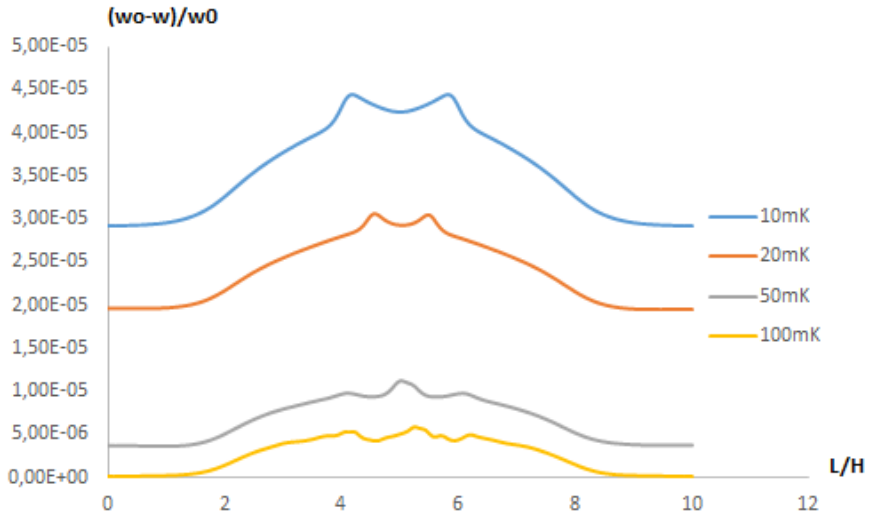

FIGURE5. Profiles of the relative mass fraction perturbation on the bottom boundary for the four ΔT (H=1 mm).

Finally, the effect of the variation of ΔT on the mass transfer at the adsorbent plate was considered. For this purpose, we calculated the mean Sherwood number on the plate. This dimensionless number, which characterizes the mass transfer at a boundary, is defined by:

$$Sh = -\int_{plate} \frac{H}{(D_{21})_i \left(w(x,0,t) - w(x,\frac{H}{2},t)\right)} D_{21} \frac{\partial w}{\partial y} dx$$

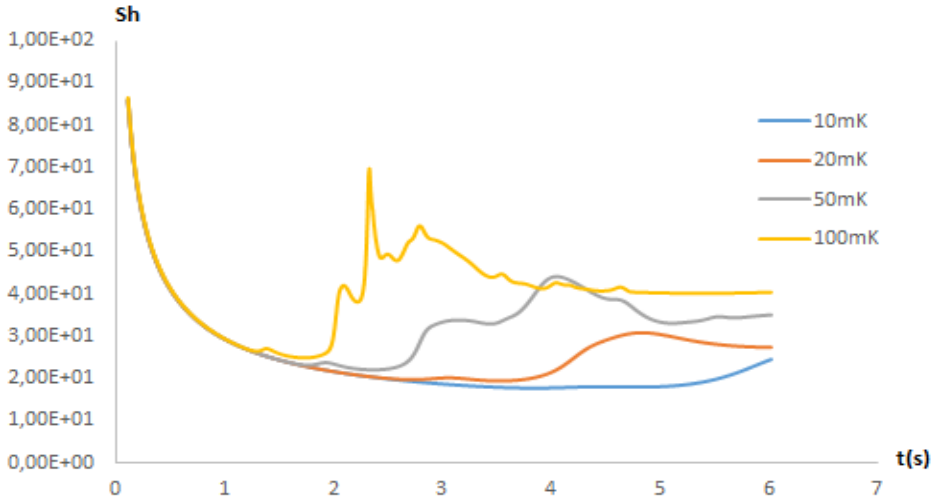

FIGURE6. Temporal evolution of the mean Sherwood number for four ΔT (H=1 mm).

Figure 6 shows the temporal evolution of the Sherwood number for the four ΔT. A strong value of Sh is observed at the very beginning of the simulations because of the increase of the plate temperature from T_i to $T_i+\Delta T$. Then, the Sherwood number rapidly decreases to reach its steady state value. The drop observed between around 2s and 3s for ΔT=100mK is due to the impact of a large cold thermal plume on the heated plate. Figure 6 reveals that the Sherwood number in the steady solution strongly increases when increasing the heating of the plate.

3.2. Influence of the height

In this section, we study the effect of confinement by decreasing the height of the cavity to H=0.5mm. The same four values of ΔT as in the previous sectionare considered.

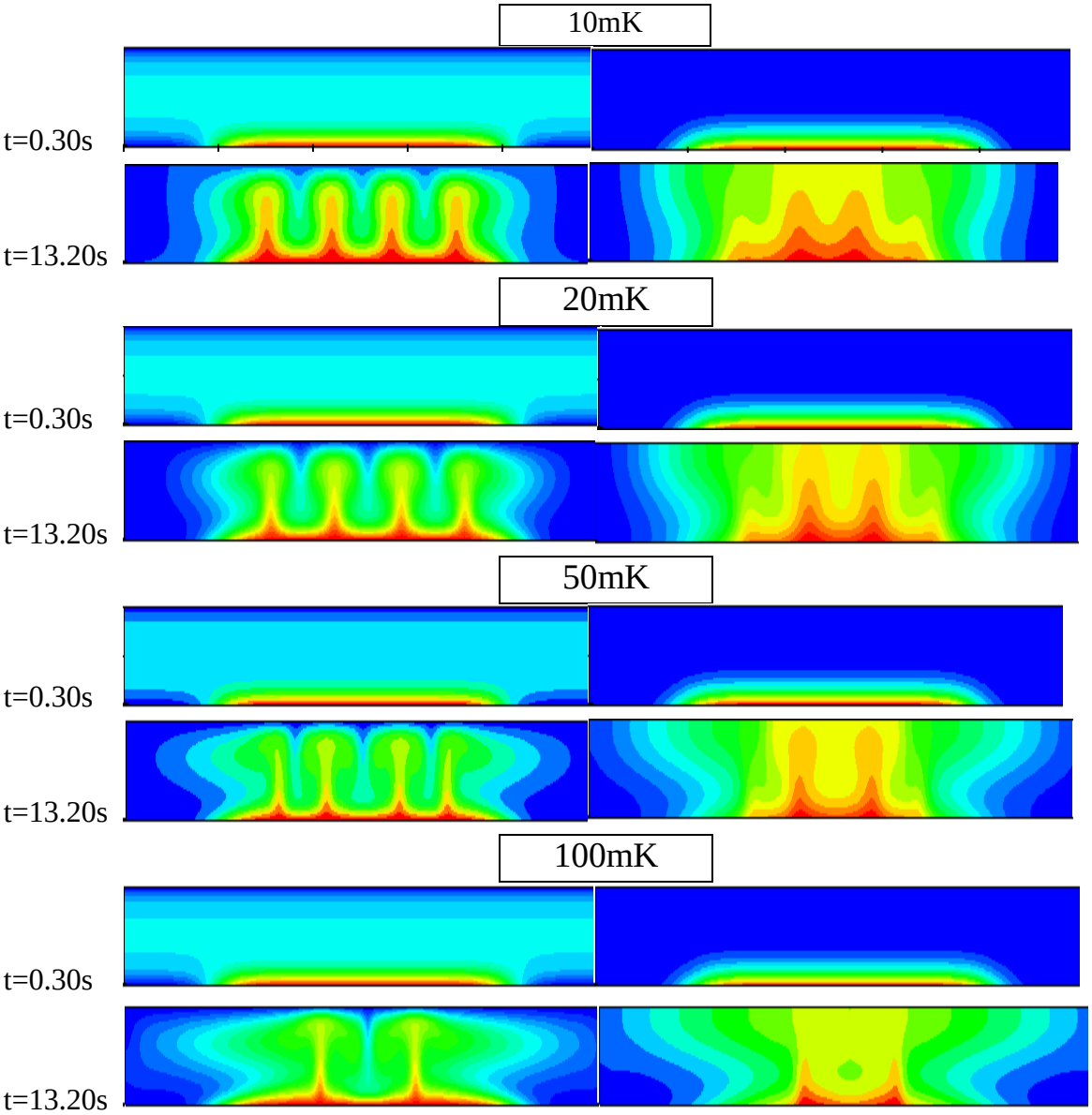

FIGURE 7. Isolines of temperature (left column) and mass fraction perturbation w-w_i (right column) for the four heated (20, 30, 50 and 100mK respectively) in the same T_i=308.15K and for H=0.5 mm.

As shown in Fig. 7, the decrease of H leads to thicker thermal and mass diffusion boundary layers. Obviously, this thickening is just due to a scale effect since the thermal diffusivity and mass diffusion coefficient only vary with the distance to the critical point. The temperature fields and the isolines of the mass fraction perturbation are clearly different from those obtained in the cavity of height H=1mm. In particular, the number of thermal plumes is multiplied by 2, except for ΔT=100mK, and mass diffusion can transfer the solute in the whole cavity. But the more important effect is that the confinement decreases the intensity of convection and regular convective cells are obtained even for the largest heating as shown in Fig. 8. This is because, for a same value of ΔT, the Rayleigh number is smaller than in the cavity of height H=1mm.

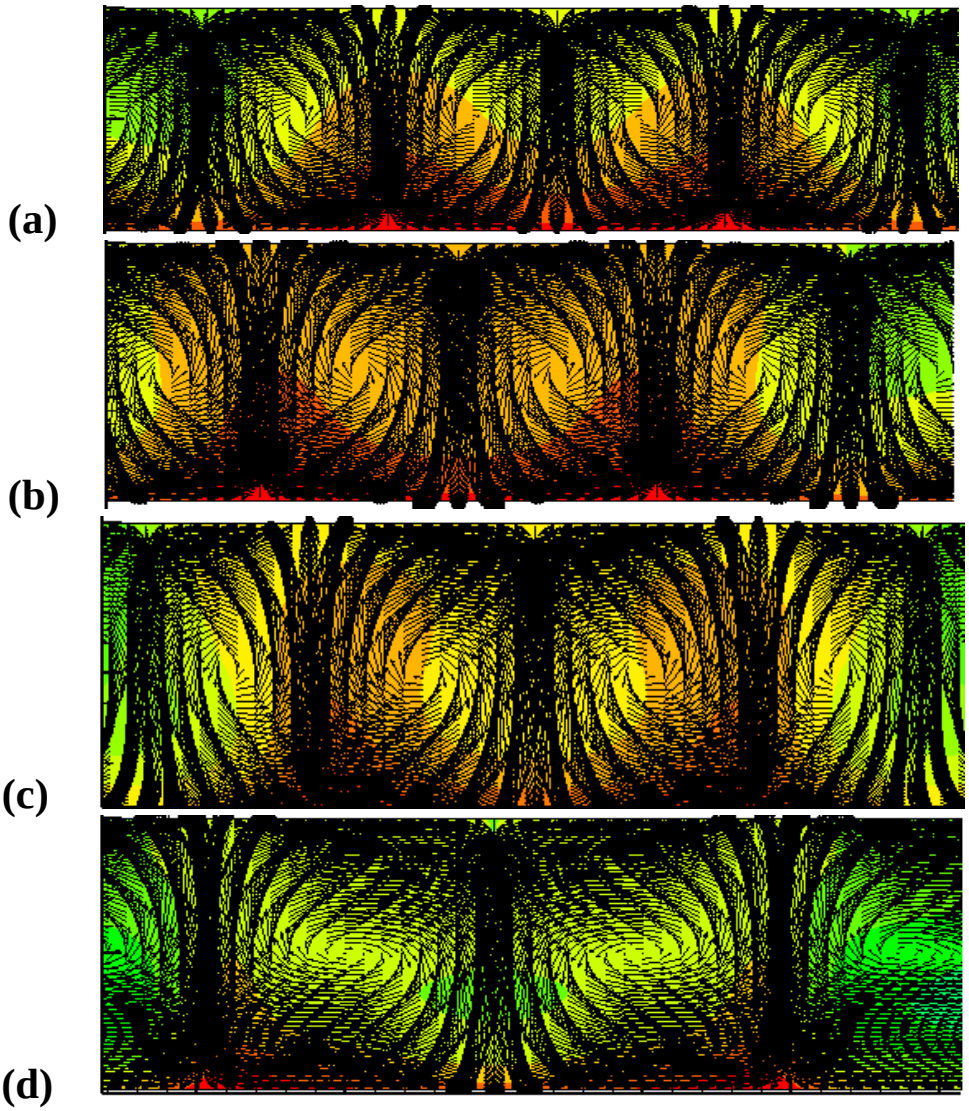

FIGURE8. Velocity field together with the isolines of w-$w_i$in the central part of the cavity (above the heated plate) for (a) ΔT=10mK, (b) ΔT=20mK, (c) ΔT=50mK and (d) ΔT=100mK, and for H=0.5 mm.

This less chaotic velocity field directly influences the profiles of the relative mass fraction perturbation $(w\text{-}w_i)/w_i$ on the bottom boundary (Fig. 9). The magnitude difference between profiles obtained with the four values of ΔT is much smaller compared to the case H=1mm (Fig. 5), and the maximum of adsorbed amount for $\Delta T \geq$20mK is larger. Therefore, in a smaller cavity, it is possible to increase the amount of solute adsorbed, which is very interesting in the framework of chemical engineering

processes. On the other hand, the profiles reveal that the adsorption of the solute is strongly inhomogeneous for all cases.

The effect of the less intense convection is also visible on the temporal evolution of the mean Sherwood number (Fig. 10). The evolution is more continuous compared with Fig. 6 but, on the other hand, the steady value is smaller than in the cavity of height H=1mm: for ΔT=50mK, we obtain Sh≈30 while Sh≈35 in the higher cavity and for ΔT=100mK, we obtain Sh≈35 while Sh≈40 in the higher cavity. Therefore, reducing the cavity height leads to a decrease of the mass transfer at the bottom plate.

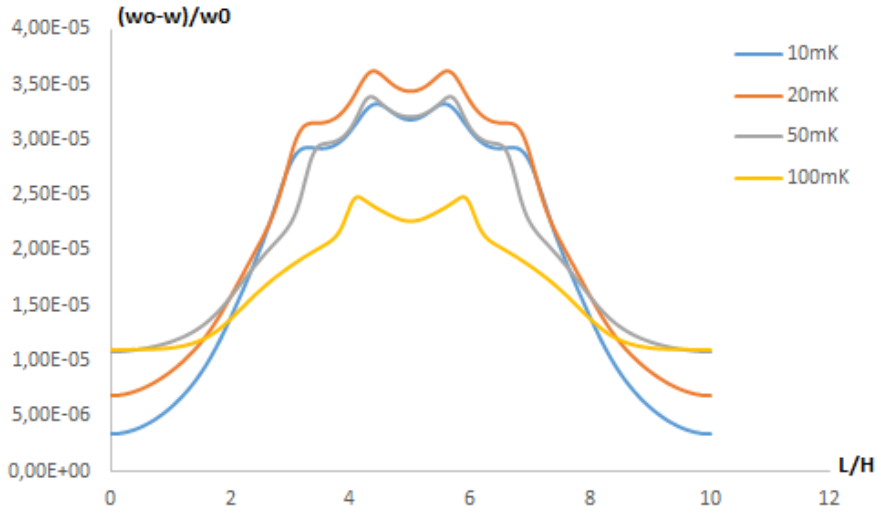

FIGURE9. Profiles of the relative mass fraction perturbation on the bottom boundary for the four ΔT (H=0.5 mm).

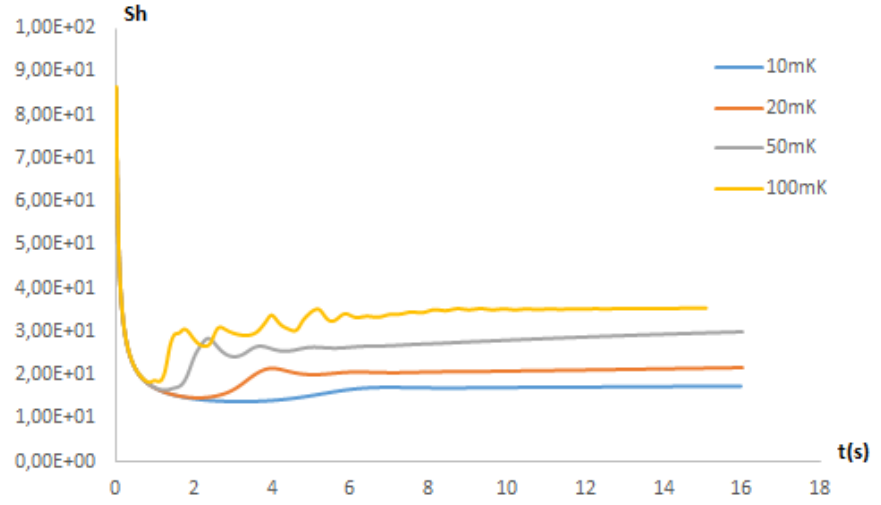

FIGURE10. Temporal evolution of the mean Sherwood number for four ΔT (H =0.5 mm).

4 Conclusion

In this paper, we presented a numerical study of heat and mass transfer in a dilute near-critical binary mixture enclosed in a rectangular cavity with a heated and adsorbent plate on the bottom boundary. The Naphthalene-CO_2 mixture was chosen as a model mixture because of the substantial experimental data on solubility of Naphthalene, allowing a correct determination of binary parameters in the mixing rules of the equation of state. However, since the diverging behavior of transport coefficients and equilibrium constant near the critical point is universal, we believe that the conclusions of our study could be applied to any binary mixture exhibiting the same kind of phase diagram. The results showed that, because of the divergence of the thermal expansion coefficient, a more homogeneous adsorption profile can be obtained when increasing the heating. However, due to the piston effect and the divergence of the derivative of the adsorption constant, the magnitude of the adsorbed amount decreases at the same time. Decreasing the cavity height reduces the decrease of the adsorbed amount of solute for large values of the heating but, on the other hand, the convection flow is less intense and leads to less homogeneous adsorption profile.

References

[1] D.D Do, H.D. Do, Adsorption of supercritical fluid in non-porous and porous carbons ; analysis of adsorbed phase volume and density,*Carbon* 41 (2003) 1777-1791.

[2] D.W. Hall, J.A. Sandrin, R.E. McBride, An overview of solvent extraction treatment technologies, *Environ. Prog.* 9 (2) (1990) 98 – 105.

[3] J.M. Becnel, K.M. Dooley, Supercritical fluid extraction of polycyclic aromatic hydrocarbon mixtures from contaminated soils, *Ind. Eng. Chem. Res*. 37 (1998) 584 – 594.

[4] A. Akgerman, C. Erkey, S.M. Ghoerishi, Supercritical Extraction of Hexachlorobenzene from Soil, *Ind Eng. Chem. Res.* 31 (1992)333-339.

[5] K.M Dooley, D. Ghonasgi, F.C. Knopf, *Environ. Prog.* 9 (1990) 197.

[6] G. Madras, C. Erkey, A. Akgerman, Supercritical extraction of organic contaminants from soil combined with adsorption onto activated carbon, *Environ. Prog.* 13 (1) (1994) 45 – 50.

[7] E. Alonso, F.J. Cantero, J. Garcia, M.J Cocero, Scale-up for a process of supercritical extraction with adsorption of solute onto active carbon. Application to soil remediation, *J. Super. Fluids* 24 (2002) 123 – 135.

[8] E. Reverchon, G. Lamberti, P. Subra, Modelling and simulation of the supercritical adsorption of complex terpene mixtures, *Chem. Eng. Sci*. 53 (1998) 3537-3544.

[9] S. Lucas, M.P Calvo, C Palencia, E. Alonso, M.J. Cocero, Mathematical Model of Supercritical CO_2 Adsorption on Activated Carbon Applied to Adsorption Scale-up, *J. of Supercritical Fluids*. 32 (2004) 193-201.

[10] I. Raspo, S. Meradji, B. Zappoli, Heterogeneous reaction induced by piston effect in supercritical binary mixtures, *Chem. Eng. Sci*. 62 (2007) 4182-4192.

[11] I. Raspo, S. Meradji; B. Zappoli, Fast mass transfer at a solid-supercritical fluid interface by piston effect, in : R. Bennacer, A.A. Mohamad, M. El Ganaoui, J. Sicard (éd.), Progress in Computational Heat and Mass Transfer (Proceedings of the 4th ICCHMT), Lavoisier, 2005, pp.132-137.

[12] M. Wannassi, I. Raspo, Numerical study of non-isothermal adsorption of Naphthalenein supercritical CO_2: Behavior near critical point, *J. Super. Fluids* 117 (2016) 203–218.

[13] I. Kikic, P. Alessi, A. Cortesi, S.J. Macnaughton, N.R. Foster, B. Spicka, An experimental study of supercritical adsorption equilibria of salicylic acid on activated carbon, *Fluid Phase Equilib*.117 (1996)304-311.

[14] M.J. Cocero, J. García, Mathematical model of supercritical extraction applied to oil seed extraction by CO2+saturated alcohol — I. Desorption model, *J. Super. Fluids* 20 (2001) 229-243.

[15] S. Paolucci, On the filtering of sound from the Navier-Stokes equation, Technical report, Sandia National Laboratores, USA, (SAND82-8257), 1982.

[16] G. Accary, I. Raspo, P. Bontoux, B. Zappoli, An adaptation of the low Mach number approximation for supercritical fluid buoyant flows, *C. R. Mec.* 331 (2005) 397–404.

[17] Y. Arai, T. Sako, Y. Takebayashi. 2002. Supercritical fluids: Molecular Interactions, Physical Properties and new Applications. Springer, Berlin.

[18] H. Higashi, Y. Iwai, Y. Takahashi, H. Uchida, Y. Arai, 1998. Diffusion coefficients of naphthalene and dimethylnaphthalene in supercritical carbon dioxide, *Fluid Phase Equilib.* 144 (1998), 269-278.